Biochimica et Biophysica Acta 1807 (2011) 11–21

Contents lists available at ScienceDirect

Biochimica et Biophysica Acta

journal homepage: www.elsevier.com/locate/bbabio

The formation of the split EPR signal from the S_3 state of Photosystem II does not involve primary charge separation

Kajsa G.V. Havelius [1], Ji-Hu Su [2], Guangye Han [3], Fikret Mamedov, Felix M. Ho *, Stenbjörn Styring *

Molecular Biomimetics, Department of Photochemistry and Molecular Science, Uppsala University, The Ångström Laboratory, P.O. Box 523, S-751 20 Uppsala, Sweden

ARTICLE INFO

Article history:
Received 27 April 2010
Received in revised form 14 September 2010
Accepted 15 September 2010
Available online 20 September 2010

Keywords:
Photosystem II
EPR
S_3 state
Near-infrared
Split signal

ABSTRACT

Metalloradical EPR signals have been found in intact Photosystem II at cryogenic temperatures. They reflect the light-driven formation of the tyrosine Z radical ($Y_Z^\bullet$) in magnetic interaction with the $CaMn_4$ cluster in a particular S state. These so-called split EPR signals, induced at cryogenic temperatures, provide means to study the otherwise transient $Y_Z^\bullet$ and to probe the S states with EPR spectroscopy. In the S_0 and S_1 states, the respective split signals are induced by illumination of the sample in the visible light range only. In the S_3 state the split EPR signal is induced irrespective of illumination wavelength within the entire 415–900 nm range (visible and near-IR region) [Su, J. H., Havelius, K. G. V., Ho, F. M., Han, G., Mamedov, F., and Styring, S. (2007) *Biochemistry 46*, 10703–10712]. An important question is whether a single mechanism can explain the induction of the Split S_3 signal across the entire wavelength range or whether wavelength-dependent mechanisms are required. In this paper we confirm that the $Y_Z^\bullet$ radical formation in the S_1 state, reflected in the Split S_1 signal, is driven by P680-centered charge separation. The situation in the S_3 state is different. In Photosystem II centers with pre-reduced quinone A (Q_A), where the P680-centered charge separation is blocked, the Split S_3 EPR signal could still be induced in the majority of the Photosystem II centers using both visible and NIR (830 nm) light. This shows that P680-centered charge separation is not involved. The amount of oxidized electron donors and reduced electron acceptors (Q_A^-) was well correlated after visible light illumination at cryogenic temperatures in the S_1 state. This was not the case in the S_3 state, where the Split S_3 EPR signal was formed in the majority of the centers in a pathway other than P680-centered charge separation. Instead, we propose that one mechanism exists over the entire wavelength interval to drive the formation of the Split S_3 signal. The origin for this, probably involving excitation of one of the Mn ions in the $CaMn_4$ cluster in Photosystem II, is discussed.

1. Introduction

Photosystem II (PSII) uses electrons derived from water to reduce the plastoquinone pool in the thylakoid membrane of higher plants, algae and cyanobacteria. During this process, protons and molecular oxygen are released into the thylakoid lumen [1–3]. Excitation of the primary electron donor P680 results in charge separation between P680 and the first electron acceptor, pheophytin, creating the charge pair $P680^+Pheo^-$. The electron is transferred from $Pheo^-$ to the quinone acceptors, first to Q_A and subsequently to Q_B. After two reductions and protonations, Q_B leaves the Q_B-pocket and diffuses into the membrane. The electron hole on $P680^+$ is reduced with an electron ultimately derived from the oxidation of water at the water oxidizing complex. The water oxidizing complex consists of the $CaMn_4$ cluster, its surrounding ligands and the redox-active tyrosine Z (Y_Z) that shuttles electrons from the $CaMn_4$ cluster to $P680^+$. The tyrosine is deprotonated upon oxidation to form a neutral radical ($Y_Z^\bullet$) [4,5]. There are also several auxiliary electron donors to $P680^+$ that come into play under different circumstances when either or both of Y_Z and the $CaMn_4$ cluster are inactive or inefficient. Y_D, a

Abbreviations: Car, carotenoid; Chl, chlorophyll; Chl_Z, secondary chlorophyll electron donor to $P680^+$; Cytb_{559}, cytochrome b_{559}; D1 and D2, the core subunits in PSII; DMSO, dimethyl sulfoxide; EPR, electron paramagnetic resonance; fl, flash; LMCT, ligand-to-metal-charge transfer; MCD, magnetic circular dichroism; MES, 2-[N-morpholino] ethanesulfonic acid; MLCT, metal-to-ligand charge transfer; NIR, near-infrared; P680, primary electron donor of PSII; Pheo, pheophytin; PpBQ, phenyl-*p*-benzoquinone; PSII, Photosystem II; Q_A and Q_B, the primary and secondary quinone electron acceptors in PSII; Y_D, Tyrosine 161 on the D2 subunit; Y_Z, Tyrosine 161 on the D1 subunit

* Corresponding authors. Tel.: +46 18 471 6580, +46 18 471 6584; fax: +46 18 471 6844.
E-mail addresses: felix.ho@fotomol.uu.se (F.M. Ho), stenbjorn.styring@fotomol.uu.se (S. Styring).
[1] Present address: Department of Physics, Freie Universität Berlin, Arnimallee 14, 14195 Berlin, Germany.
[2] Present address: Department of Modern Physics, University of Science and Technology of China, Hefei, Anhui, 230026, China.
[3] Present address: Department of Chemistry, Umeå University, 901 87 Umeå, Sweden.

0005-2728/$ – see front matter © 2010 Elsevier B.V. All rights reserved.
doi:10.1016/j.bbabio.2010.09.006

homologously located tyrosine-residue on the D2 subunit, can in its reduced form reduce $P680^+$ [6]. Carotenoid, Chl_Z and Cytb_{559} may also feed in electrons to reduce $P680^+$ [7–9]. However, only electron donation from Y_Z and the $CaMn_4$ cluster leads to water oxidation.

To form one molecule of oxygen, the $CaMn_4$ cluster cycles through five intermediate oxidation states, S_0 to S_4. This is known as the S state cycle. The most reduced state in the S state cycle is the S_0 state, while the S_1 state is the dark-stable state. The subsequent states S_2 and S_3 are metastable intermediates that decay back to the S_1 state in the seconds to minutes timescale if allowed to dark-adapt [10]. The last transition to complete the cycle, the $S_3 \rightarrow [S_4] \rightarrow S_0$ transition, involves the production of O_2.

During the electron transfer reactions on the donor side of PSII, Y_Z is only transiently found in its oxidized radical state, $Y_Z^{\bullet}$. Y_Z is oxidized by $P680^+$ in the ns–μs time regime [11] and the $Y_Z^{\bullet}$ formed is reduced by the $CaMn_4$ cluster within μs–1 ms [12]. The exact kinetics depend on the redox state of the $CaMn_4$ cluster and the H-bonding network around Y_Z. The transient nature of $Y_Z^{\bullet}$ makes the radical difficult to approach with spectroscopy and there is limited knowledge about the molecular interactions of $Y_Z^{\bullet}$ with the $CaMn_4$ cluster and other species in its vicinity. This changed with the discovery that a radical, thought to be $Y_Z^{\bullet}$, can be formed by illumination of PSII in the frozen state [13,14]. At very low temperatures (5–20 K) the result is a series of EPR signals reflecting the magnetic interaction between the radical ($Y_Z^{\bullet}$) and the $CaMn_4$ cluster [15]. These EPR signals are S state-dependent and provide new spectroscopic probes of both $Y_Z^{\bullet}$ and the $CaMn_4$ cluster. In the S_0, S_1 and S_3 states can magnetic interaction EPR signals (better known as "split signals") be induced by visible light between 415 and 690 nm [16]. This is generally thought to reflect Y_Z oxidation (in the particular S state) driven by photosynthetic charge separation involving P680, Pheo and Q_A.

However, in the S_2 and S_3 states split EPR signals can also be induced by near-infrared (NIR) light [17,18]. The wavelength dependence has been described for the S_3 state and stretches to 900 nm [16,19], clearly out of reach for photosynthetic charge separation, which is known to be inactive above 730 nm at the very low temperatures used [20]. It was previously thought that only NIR illumination and not visible light illumination could induce the split EPR signal in the S_3 state [17,21,22]. However, recently [16] we demonstrated that the Split S_3 EPR signal can be induced by monochromatic light in the spectral range 415–900 nm. Furthermore, all studied aspects of the Split S_3 signal are similar, regardless of whether it is induced by visible light or by NIR light [16]. This is interesting as the mechanism for the induction of the Split S_3 signal in the visible and in the NIR ranges might differ.

Here we investigate whether a single light-induced mechanism leads to oxidation of Y_Z resulting in the formation of the Split S_3 signal in the visible spectral range (415–730 nm) as well as in the near-infrared region (740–900 nm). If this is the case, the species absorbing in the NIR must also have an appreciable absorption spectrum extending over the entire visible spectrum. If different mechanisms apply, Y_Z would presumably be oxidized by $P680^+$ in the visible part of the spectrum (415–730 nm) and by an alternative species in the NIR. In this paper we present strong experimental evidence against Y_Z being oxidized by $P680^+$ at 5 K when the OEC is in the S_3 state. Instead our data support a single mechanism of induction of the Split S_3 EPR signal to apply in the whole spectral region (415–900 nm) [16].

2. Materials and methods

2.1. PSII membrane preparation

PSII-enriched membranes (BBY membranes) were prepared from hydroponically grown spinach (*Spinacia oleracea*) according to [23] with modifications [24] using a mild detergent protocol and stored at 6 mg Chl/ml at −80 °C. The storage-buffer was 25 mM MES-NaOH (pH 6.1), 15 mM NaCl, 3 mM $MgCl_2$ and 400 mM sucrose. Chl determinations were made according to Arnon [25]. Steady-state oxygen evolution at 20 °C was 350 ± 50 μmol O_2 (mg Chl)$^{-1}$ h^{-1} measured with a Clark-type electrode at 10 μg Chl/ml in a buffer with 20 mM MES-NaOH (pH 6.1), 10 mM NaCl, 10 mM $MgCl_2$, 5 mM $CaCl_2$ and 400 mM sucrose and with 0.5 mM P*p*BQ (from stock 50 mM in DMSO) as electron acceptor. All EPR measurements were performed in samples with ~3 mg Chl/ml.

2.2. Flash advancement to the S_3 state

BBY membranes (3 mg/ml) in calibrated EPR tubes were exposed to room light for a few minutes to fully oxidize Y_D and then dark-adapted for 30 min. The samples were given 1 saturating laser flash and then dark-adapted for 15 min at 20 °C to synchronize PSII to the dark-stable S_1 state [26]. P*p*BQ (50 mM in DMSO) was then added to the sample to a final concentration of 1 mM. S_1 state samples (0 flash) were frozen at this stage. For advancement to the S_3 state, the sample was given 2 saturating laser flashes (Nd:YAG laser operating at 5 Hz, 6 ns, 532 nm, 400 mJ/pulse) at 2 °C, and frozen in an ethanol/dry ice bath within 1–2 s after flashing. The typical S state composition of the 2-flash sample was ~68% S_3 and ~32% S_2 state centers as calculated from the yield of the S_2 multiline signal [27].

2.3. EPR spectroscopy

Low-temperature EPR measurements were performed in the dark with a Bruker ELEXSYS E500 spectrometer using a SuperX EPR049 microwave bridge and a Bruker 4122SHQE super high-Q cavity. The system was fitted with an Oxford 900-crystat and an ITC-503 temperature controller from Oxford instruments Ltd. The split EPR signals and the other radical EPR signals were induced by illumination directly into the cavity at 5–7 K. For NIR illumination, the light at 830 nm was provided by a LQC830-135E continuous laser diode (Newport, USA) (67 W/m^2 at the position of the cavity window). Visible light illumination was provided by a Universal Flexilux 150 HL lamp connected to a fiberoptics light guide (Schölly, Gemany, 280 W/m^2) or a slide projector fitted with a $CuSO_4$ (aq) filter and a plexiglas light guide (20 W/m^2). Incubation in complete darkness at 5–10 K after the 830 nm or visible light illuminations was executed for the times indicated. Unless otherwise indicated, the split signals are presented as (illumination − dark) difference spectra.

2.4. Pre-reduction of Q_A and quantification of EPR signals

In some experiments the effect of pre-formed Q_A^- on the formation of the split signal was investigated. In such experiments, Q_A^- was first induced in the sample to 70–90% by illumination for 25 min at 77 K with two 800-W projector lamps focused on the EPR sample. $CuSO_4$ (aq) filters were used to filter out NIR light. These samples with pre-reduced Q_A^- were then used for respective split signal induction experiments.

For the quantification of Q_A^-, the amplitude of the Q_A^--Fe^{2+} EPR signal ($g = 1.87$, also used in [28]) of a given sample was compared to the maximum photo-inducible Q_A^--Fe^{2+} EPR signal from a sample first illuminated at 77 K and thereafter illuminated at 5 K. This two-stage illumination protocol was used to account for the decay of a fraction of Q_A^- during the 77 K illumination and subsequent transfer to the EPR spectrometer. Contributions from the radicals of oxidized carotenoid (Car^+) or chlorophylls (Chl^+) were quantified by double integration of their non-saturated EPR spectra and comparison to the spectrum of the fully oxidized $Y_D^{\bullet}$ (1 spin/PSII) measured in the same sample. Quantification of the oxidized Cytb_{559} was estimated from comparison of its EPR spectrum (the g_z peak) with the spectrum from fully oxidized Cytb_{559} in a sample illuminated at 77 K. This treatment is

considered to result in oxidized Cytb_{559} in 100% of the PSII centers [29]. In our BBY samples, ~60% of Cytb_{559} are in the reduced high-potential from the start, and all available reduced Cytb_{559} could be photo-oxidized. [30–32].

3. Results

Using well-defined laser flashes, we have shown [16] that the Split S_3 EPR signal can be induced in the S_3 state by illumination at 5 K in a

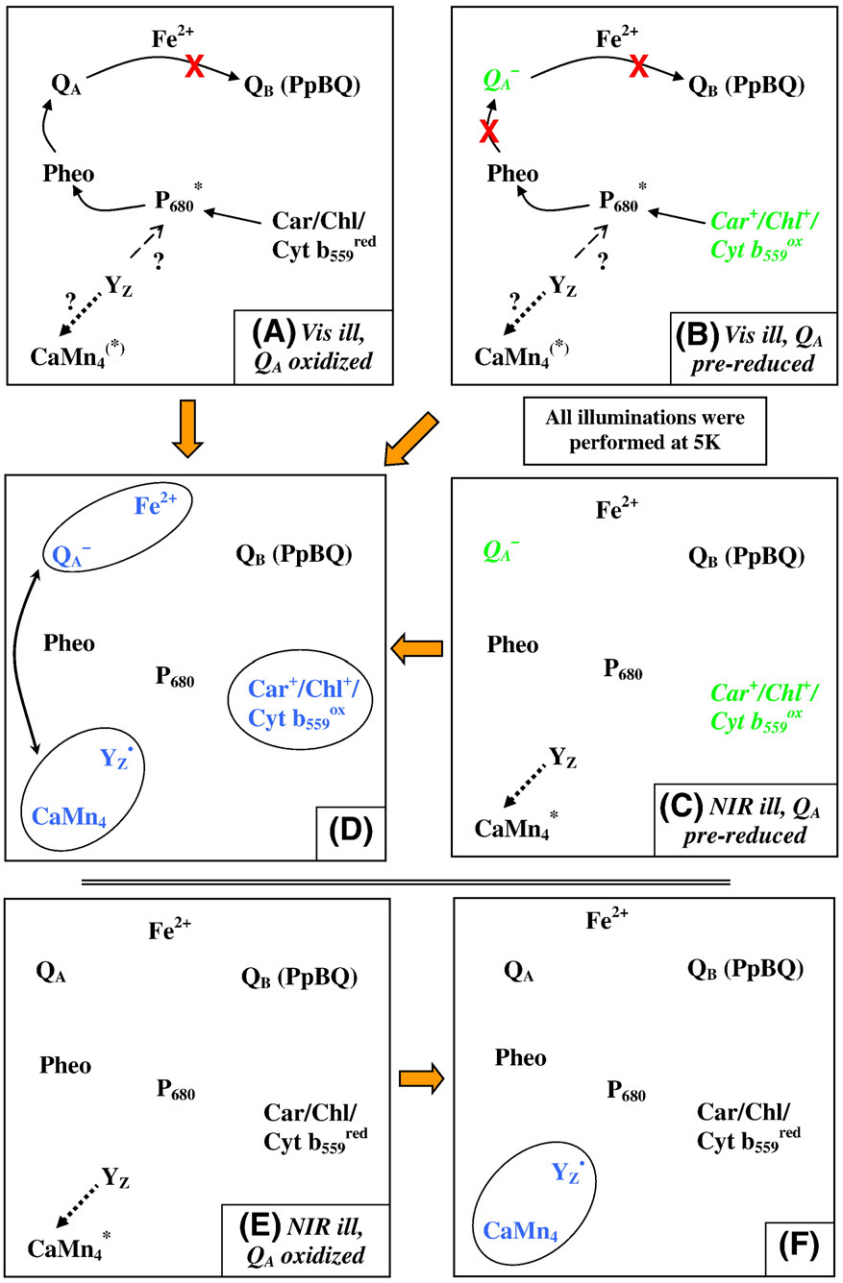

Scheme 1. Induction of the Split S_3 signal and associated cryogenic electron transfer processes. Species measured in this study by EPR spectroscopy after split signal induction by illumination at 5 K are marked with ovals, and species reduced or oxidized as a result of 77 K illumination are *in green* [30,33]. Oxidation of Y_Z to give $Y_Z^{\bullet}$ yields the interacting $CaMn_4$ cluster/$Y_Z^{\bullet}$ pair that leads to the Split S_3 signal. Two possible mechanisms for the oxidation of Y_Z under visible light illumination are considered here: the P680-driven mechanism refers to oxidation of Y_Z by $P680^+$ (dashed arrows), and the Mn-centered mechanism refers to oxidation of Y_Z by an excited $CaMn_4$ cluster (dotted arrows). Panels (A) & (D): Visible illumination of PSII at 5 K leads to P680-centered charge separation. Where Q_A is in its oxidized state, the excited P680 donates an electron to Q_A via Pheo. The Q_A^- species can be detected by the Q_A^--Fe^{2+} EPR signal [34]. At such low temperatures, however, further electron transfer to Q_B (or the added electron acceptor PpBQ occupying the Q_B site) is blocked [35–37]. The resulting $P680^+$ can be re-reduced by Car, Chl or Cytb_{559} [33], the oxidized forms of which can be detected by EPR spectroscopy [34]. Y_Z is also a potential donor to $P680^+$. Therefore, the total amount of Car/Chl/Cytb_{559} oxidized by 5 K illumination reflects the extent to which Y_Z contributes to $P680^+$ re-reduction, and thereby the extent to which the Mn-centered mechanism is responsible for Split S_3 signal induction. Irrespective of the mechanism for Y_Z oxidation, the recombination partner of the split signal $CaMn_4$ cluster/$Y_Z^{\bullet}$ pair is Q_A^- (doubled-headed arrow in panel (D)) [28]. Panels (B), (C), & (D): Where 77 K illumination is used, a large proportion (~70%) of Q_A is pre-reduced to the Q_A^- state prior to split signal induction at 5 K. The donor species during 77 K illumination are again Car/Chl/Cytb_{559}. For subsequent visible light illumination at 5 K (panel (B)), oxidation of Y_Z by $P680^+$ remains a possibility, but only in those "open" centers where Q_A remained oxidized after 77 K illumination. Centers with Q_A^- are closed to stable P680-centered charge separation, and thus only the Mn-centered mechanism is available for induction of the Split S_3 signal. By contrast, NIR illumination at 5 K leads only to excitation of the $CaMn_4$ cluster. The Mn-centered mechanism is therefore the only available pathway for the generation of $Y_Z^{\bullet}$ and hence the Split S_3 signal. Again, Q_A^- is the recombination partner of the split signal $CaMn_4$ cluster/$Y_Z^{\bullet}$ pair. Panels (E) & (F): Where Q_A was not pre-reduced prior to NIR light illumination at 5 K, the Mn-centered mechanism is the only option for $Y_Z^{\bullet}$ and thereby Split S_3 signal induction. Since no P680-driven charge separation has taken place, there is no recombination partner for the resulting $CaMn_4/Y_Z^{\bullet}$ pair available.

wide spectral range between 415 and 900 nm, and not only by light in the near-infrared region as first proposed [17]. A question remaining from the previous study is whether a single mechanism can explain the induction of the Split S_3 signal across the entire wavelength range, or whether wavelength-dependent mechanisms are required. This is investigated here. To facilitate understanding of our experimental design, the relevant processes that take place under the cryogenic experimental conditions that were employed in this study are summarized in Scheme 1.

3.1. Induction of the Split S_3 signal by visible and NIR illumination

The Split S_3 signals induced by visible and NIR illuminations are shown in Fig. 1A. The signal induced by illumination by NIR light is characterized by a large double trough around 3400 G, a smaller trough at 3345 G and a peak centered at 3200 G (Fig. 1A, black spectrum). The shape of the Split S_3 signal induced by visible light is different from that of the NIR-induced signal, with the presence of an additional signal due to the presence of Q_A^--Fe^{2+}. This EPR signal can be isolated by subtraction of the NIR-induced Split S_3 signal from the EPR spectrum induced by visible light. The resulting spectrum (Fig. 1A, dotted spectrum) shows a typical Q_A^--Fe^{2+} signal that is recognizable by the trough at 3560 G, consistent with literature reports of this signal [28,34]. The presence of this signal reflects the fact that visible illumination drives charge separation at P680, leading to the formation of the Q_A^--Fe^{2+} species [28,38,39]. Under cryogenic conditions, such as those used for Split signal induction, where forward electron transfer from Q_A to Q_B is not possible, such Q_A^- containing centers are "closed" and P680-centered charged separation is blocked until Q_A^- is re-oxidized through charge recombination. By contrast, since NIR illumination (830 nm here) is unable to excite P680, there is an absence of Q_A^- formation arising from P680-centered charge separation, and such centers containing (oxidized) Q_A remain "open". This can also be observed in EPR spectra taken over a wider magnetic field range (Fig. 2). The reduction of Q_A and an accompanying oxidation of Cytb_{559}, a side-path electron donor can be clearly seen in the case of visible light illumination [33,34], but not where NIR illumination was used (though interestingly, a $g\sim5$ signal was seen in both samples; discussed further later). This is again consistent with the lack of P680 excitation by NIR light. These are crucial differences between the effects of the two illumination regimes, and are used later to investigate the origins of the Split S_3 signal.

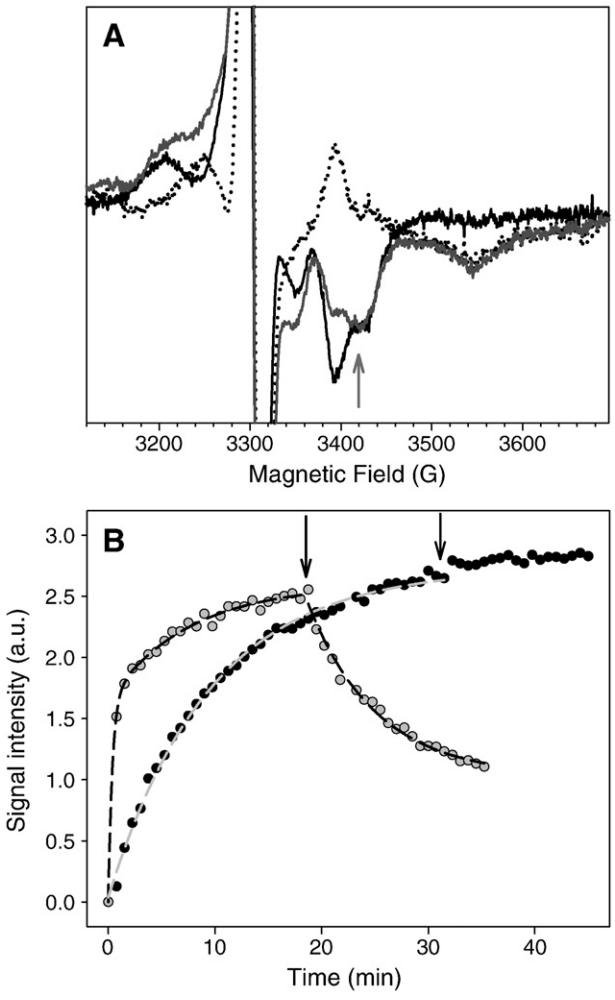

Fig. 1. Induction of the Split S_3 EPR signal by illumination of PSII centers in the S_3 state at 5 K in the absence of pre-formed Q_A^-. (A) The Split S_3 signal EPR spectrum ((during illumination − before illumination) difference spectrum) induced at 5 K by 32 min NIR illumination (black line) and by 19 min visible light illumination (grey line). The dotted line is the difference spectrum between the visible- (280 W/m^2, grey) and NIR-induced (830 nm, 67 W/m^2, black) signal spectra. (B) Time course of the induction and decay of the Split S_3 EPR signal by illumination at 5 K with visible light (grey circles) or NIR light (black circles). The induction kinetics was followed until maximum signal intensity was reached, at which point the light was turned off (arrows). The decay kinetics after the different illumination regimes were followed in the dark. Each data point represents the signal intensity at 3420 G (arrow in A) measured in a field swept spectrum recorded with 45 second intervals. The lines in the decay phases represent fitting to single exponential decay kinetics (see Table 1). EPR conditions: temperature 5 K, microwave frequency 9.27 GHz, microwave power 25 mW, modulation frequency 100 kHz, and modulation amplitude 10 G. The amplitude of $Y_D^\bullet$ was used as an internal standard in each sample.

3.2. Induction and decay kinetics of the Split S_3 signal without pre-formed Q_A^-

To study the induction and decay behavior of the Split S_3 signal in centers with Q_A in its oxidized state, PSII was illuminated at 5 K in the

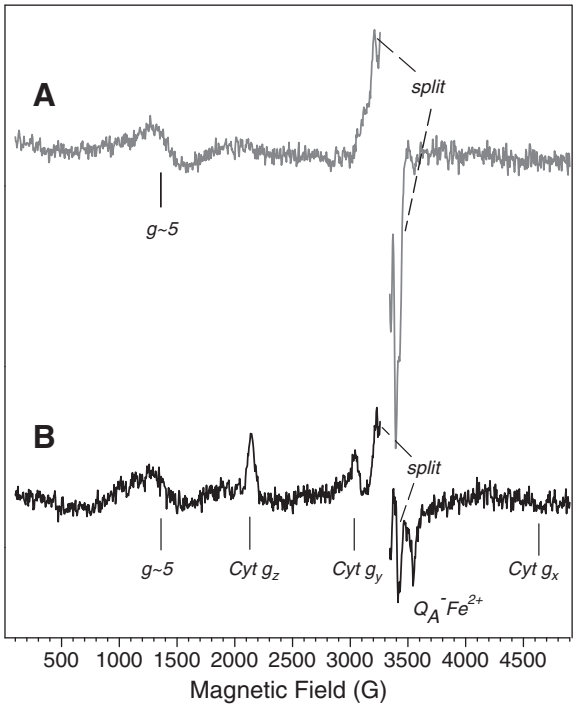

Fig. 2. The stable light-induced EPR signals formed in the S_3 state samples without pre-formed Q_A^- upon illumination at 5 K with (A) NIR or (B) visible light illumination. Difference spectra (illuminated *and* dark-adapted minus before illumination). In (A) the Split S_3 signal and the $g\sim5$ signal are marked. In (B), the Split S_3 signal, the $g\sim5$ signal, the three components of the oxidized Cytb_{559} signal, and the Q_A^--Fe^{2+} signal (solid bar) are marked. EPR conditions: temperature 10 K, microwave power 5 mW, and modulation amplitude 10 G.

S_3 state with either NIR or visible light until the split EPR signal spectrum stopped increasing in intensity (Fig. 1B). At 3420 G (Fig. 1A, grey arrow) the contributions from the overlapping Q_A^--Fe^{2+} spectrum are minimal. Therefore, the intensities of NIR-induced and visible-induced Split S_3 signals can be compared at this field position, despite the different light used for the induction.

The half time for reaching maximum signal intensity of the NIR-induced signal (Fig. 1B, black circles) was 384 s and the maximal signal size was obtained after ca. 32 min illumination. On the other hand, the visible light-induced signal (Fig. 1B, grey circles) was induced within tens of seconds, with the maximal amplitude being reached after ca. 19 min. In both cases, approximately the same Split S_3 signal amplitude was obtained. The maximal signal induced by visible light induction was 96% that induced by NIR light. We conclude therefore that both illumination regimes are able to induce the Split S_3 signal to an equal level.

By contrast, the decay kinetics are completely different between the two illumination regimes. Whereas the signal induced by NIR light was stable in the dark at 5 K for at least 1 h after the light was turned off (Fig. 1B, black circles after the arrow), the Split S_3 signal induced by visible light was unstable in the dark. It decayed to ~42% of its original amplitude with a decay half time of 270 s under the same conditions (Fig. 1B, grey circles).

3.3. Induction and decay kinetics of the Split S_3 signal in the presence of pre-formed Q_A^-

As noted earlier, PSII centers containing Q_A^- are closed to further P680-centered charge separation. Consequently, P680 in such centers would also be unable to drive the oxidation of Y_Z to give the split signal forming radical $Y_Z^\bullet$. Therefore, if split signal formation originates solely from P680-centered charge separation, split signal intensities should always decrease in proportion to the amount of closed, Q_A^--containing PSII centers in the sample.

This was tested for the Split S_3 signal using PSII samples in the S_3 state in which Q_A^- was pre-formed by means of illumination at 77 K (see Materials and methods). Fig. 3A shows the EPR signals induced in samples predominately in the $S_3Q_A^-$ state, directly after illumination with NIR or visible light at 5 K (black and grey lines in Fig. 3A, respectively). Compared to the spectra in Fig. 1A, where Q_A was not pre-reduced, the NIR and visible light illuminations of Q_A^--containing samples give EPR spectra that are much more similar to each other. This was due to the formation of a significantly smaller Q_A^--Fe^{2+} EPR signal (Fig. 3A, dotted line) in the sample exposed to visible light. This is expected, due to the presence of a large fraction of closed PSII centers containing Q_A^- to begin with. The illumination protocol used for reducing Q_A at 77 K prior to split signal induction gave rise to Q_A^- in ~70% of the sample. This is reflected in the reduction in the Q_A^--Fe^{2+} EPR signal induced by the visible illumination to ~30% of the maximally inducible signal. As expected, the spectral shape of the NIR-induced split signal remains unchanged, since NIR light does not drive P680-centered charge separation regardless of whether Q_A is oxidized or reduced.

Despite a majority of PSII centers being closed to P680-centered charge separation due to the presence of Q_A^-, the intensity of the Split S_3 signals induced by NIR and visible light illumination remained very high (Fig. 3). The amplitude of the Split S_3 signals reached 74% (NIR) and 86% (visible) of the maximum Split S_3 signal induced by NIR light in the absence of Q_A^- (Fig. 3B). Thus we can conclude that the presence of pre-reduced Q_A in the majority of PSII (~70%) did not prevent the formation of the Split S_3 signal to any major extent, neither when it was formed by visible nor when it was formed by NIR illumination. Most significantly, comparing the samples with and without pre-formed Q_A^-, the decrease in the intensity of the Split S_3 signal induced by visible light did not correlate with the increase in the number of centers containing pre-formed Q_A^-. The reduction of this signal from

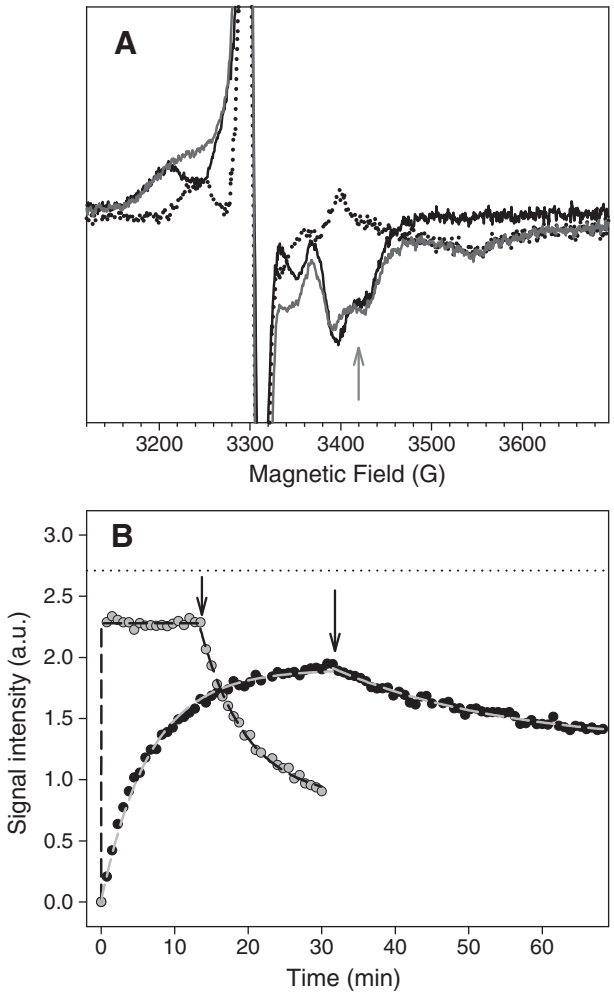

Fig. 3. Induction of the Split S_3 EPR signal by illumination of PSII centers in the S_3 state at 5 K in the presence of pre-formed Q_A^- in ~70% of centers. Pre-reduction of Q_A was performed by illumination at 77 K prior to split signal induction at 5 K (see Materials and methods). (A) The Split S_3 signal EPR spectrum ((during illumination − before illumination) difference spectrum) induced by 32 min NIR illumination (830 nm, 67 W/m^2, black line) and a spectrum induced by 13 min visible light (280 W/m^2, grey line) in the presence of pre-formed Q_A^-. The dotted spectrum is the (visible − NIR) difference spectrum. (B) Time course of the induction and decay of the Split S_3 EPR signal by illumination at 5 K with visible light (grey circles) or NIR light (black circles). The rise kinetics of the signal was followed until a stable signal amplitude was reached. The dotted line reflects the maximal amplitude of the Split S_3 signal in the absence of pre-formed Q_A^- (from Fig. 1B). The light was turned off (arrows) and the decay of the Split S_3 signal in the dark was followed. Each data point represents the signal intensity at 3420 G measured in a field swept spectrum recorded with 45 second intervals. The lines in the decay phases represent fitting to single exponential decay kinetics (see Table 1). EPR conditions as in Fig. 1.

98% to 86% of the maximum inducible intensity is much less than what would have been expected from a sample where ~70% of the centers are now closed to P680-centered charged separation. As discussed earlier, if Split S_3 signal formation would solely originate from charge separation from P680, these changes should correlate. This lack of correlation was therefore the first indication that the mechanism behind the induction of the Split S_3 signal may be independent of charge separation originating from P680.

Apart from the maximum inducible intensity of the Split S_3 signals, the kinetics of the induction and decay of the signal were also affected by the oxidation state of Q_A.

The NIR-induced Split S_3 signal had similar though different rise kinetics both in the absence and presence of Q_A^- ($t_{1/2} = 384 \pm 16$ and 268 ± 13 s, respectively; Figs. 1B and 3B). By contrast, the kinetics of the decay of these signals in the dark at 5 K were totally different

depending on the redox state of Q_A^-. As observed before [16,40], the NIR-induced split signal was stable in the dark at 5 K in the absence of Q_A^- (Fig. 1B). However, when Q_A^- was present from the start in ~70% of the PSII centers, 34% of the Split S_3 signal decayed with $t_{1/2} = 960$ s. The rest of the signal was stable during the timeframe of our EPR measurement (Fig. 3B). This is an important result which clearly shows that the radical species ($Y_Z^\bullet$) induced in the Split S_3 EPR signal recombines with Q_A^-, even when the split signal itself was generated through NIR illumination, and therefore independent of Q_A^- formation. Based on this observation that Q_A^- is the recombination partner of the Split S_3 signal radical ($Y_Z^\bullet$), and similar to what has been demonstrated for the Split S_1 signal [18,28,41], an estimate of the Split S_3 signal on a PSII basis could be made by quantifying the re-oxidation of Q_A^- that accompanied the decay of the Split S_3 signal. This was done by measuring the Q_A^--Fe^{2+} signal intensity before induction of the Split S_3 signal, and after its decay in the dark. By doing so, it was found that the Split S_3 signal was induced in about 50% of PSII centers.

For the Split S_3 signal induced by visible light, the rise kinetics were in contrast quite dependent on the redox status of Q_A. The rise of the Split S_3 signal in the presence of Q_A^- was much faster than in its absence. In the presence of Q_A^-, the Split S_3 signal reached its maximum size in less than 1 min, with the major part of the signal being formed within two time points (i.e. 45 s; Fig. 3B). In the absence of Q_A^-, however, the rise time was slower and biphasic (Fig. 1B), with only ~60% of the Split S_3 signal being induced during the first 45 s of illumination ($t_{1/2} = 16 \pm 4$ s in 64 ± 3% of centers for this phase according to a bi-exponential fitting of the data).

Finally, the Split S_3 EPR signal induced by visible light was found to partially decay in the dark, with $t_{1/2} = 270$ s. This kinetic behavior was found both when Q_A was oxidized and reduced (Q_A^-) from the start (Figs. 1B and 3B). However, somewhat more of the Split S_3 signal decayed in the presence of pre-formed Q_A^- (64%) than in its absence (58%).

Table 1 summarizes the induction and decay results from the Split S_3 EPR signal under the different conditions mentioned earlier.

Table 1
Quantification of light-induced EPR signals at 5 K in PSII centers in the S_3 state in the absence or presence of pre-formed Q_A^-. Illumination was provided with NIR light (67 W/m^2) or visible light (280 W/m^2).

		NIR illumination		Visible light illumination	
		Q_A not pre-reduced	Pre-reduced Q_A[a]	Q_A not pre-reduced	Pre-reduced Q_A[a]
Q_A^--Fe^{2+}	Before illumination at 5 K (%)[b]	0	70	0	70
	Induction at 5 K (%)[b]	0	0	90	30
Split S_3	Signal amplitude (% of maximum inducible)[c]	100	74	96	86
	Half rise time; $t_{1/2}$ (s)[d]	384 ± 16	268 ± 13	16 ± 4 and 314 ± 93	N.R.[e]
	Rise (% of amplitude)	100	100	64 ± 3 and 36 ± 3	100
	Half decay time; $t_{1/2}$ (s)[f]	Stable	960	270	270
	Decay (% of amplitude)	0	34	58	64

[a] Q_A pre-reduced by extensive illumination at 77 K.
[b] The maximum EPR signal from Q_A^--Fe^{2+} is set to represent reduced Q_A in 100% of PSII and was obtained in the sample illuminated *both* at 77 K and 5 K.
[c] The maximum Split S_3 signal amplitude was obtained with NIR illumination of a sample without pre-formed Q_A^-. This amplitude was set as 100%.
[d] Half time to reach the maximal signal size. Errors are based on curve fitting of the data points to exponential rise to maximum functions.
[e] N.R.: not resolved (far below our time resolution).
[f] Half time for decay of the signal during incubation in the dark at 5 K. The decay half time was obtained from fitting the data in Figs. 1B and 3B to a single exponential decay.

3.4. Comparisons with the Split S_1 signal induced in the presence or absence of pre-reduced Q_A

With respect to the mechanism underlying the induction of the Split S_3 signal with or without pre-reduced Q_A, a particularly illuminating comparison can be made with corresponding inductions of the Split S_1 signal.

The Split S_1 signal has been well-studied, and it has been demonstrated that it arises from the interaction of the $CaMn_4$ in the S_1 state with the $Y_Z^\bullet$ radical species formed as a result of P680-centered charge separation [14,28,42]. The induction and decay behavior of this signal correlates with the formation and decay of Q_A^- [28], and a tyrosine radical spectrum with enhanced relaxation properties has been observed in conjunction with the induction of the Split S_1 signal [41,43–45]. Unlike the Split S_3 signal, it can only be induced by light in the visible region [16].

The Split S_1 spectrum induced by visible illumination in samples poised in the S_1 state in the presence and absence of pre-formed Q_A^- is shown in Fig. 4A (grey and black, respectively). It is clearly seen that where Q_A^- was first induced by 77 K illumination prior to the split signal inducing illumination at 5 K, there is a significant drop in the

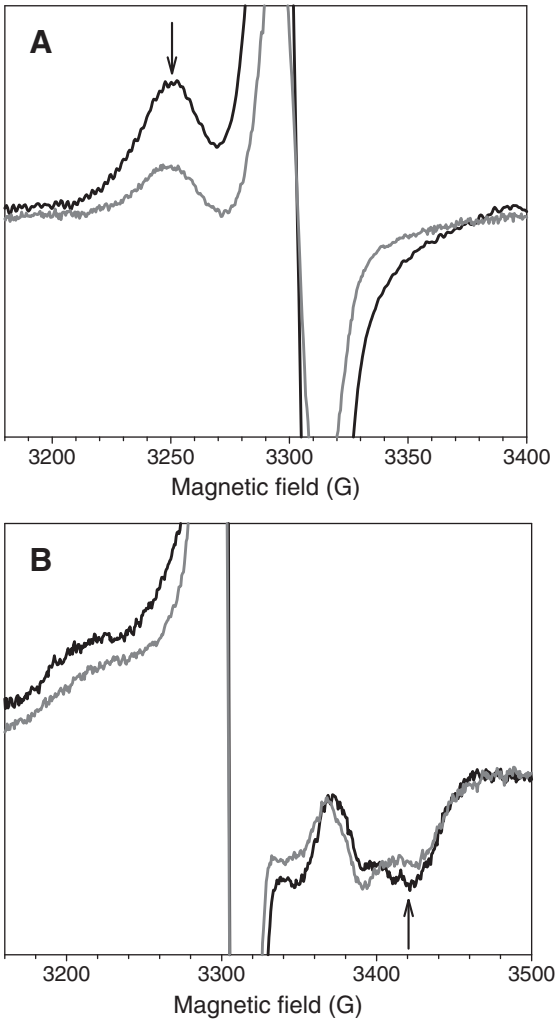

Fig. 4. Comparisons of the Split S_1 and Split S_3 signals induced by visible illumination at 5 K in the presence and absence of pre-formed Q_A^-. (A) The Split S_1 signal (arrow) induced in the absence (black) and presence (grey) of pre-formed Q_A^-. Reduction of Q_A^- was performed by visible light illumination at 77 K prior to the 5 K split signal induction illumination. (B) The Split S_3 signal (arrow) induced in the absence (black) and presence (grey) of pre-formed Q_A^-. (These have been replotted from Figs. 1A and 3A, for ease of direct comparison.) EPR conditions as in Fig. 1. S_1 and S_3 signals were induced to maximum intensity with visible light, 20 and 280 W/m^2, respectively.

yield of the Split S_1 signal obtained. The signal intensity is reduced to 35% of the signal induced without pre-formed Q_A^-. This marked drop in split signal intensity due to the presence of centers closed to further charge separation is what is expected of a signal induction mechanism centered at P680.

Fig. 4B presents a corresponding comparison of the intensities of the Split S_3 signal induced with or without prior reduction of Q_A. In stark contrast to the behavior of the Split S_1 signal, there was only a minor reduction in the intensity of the Split S_3 signal. Clearly, the intensity of this signal is far from correlated to the amount of Q_A^- centers present. This is not expected from a signal induction mechanism based on P680-centered charge separation. Taken together with the behavior of the Split S_1 signal induction under corresponding conditions, and the fact that the Split S_3 signal can also be induced by NIR radiation, there is strong evidence that the mechanism for the formation of Split S_3 signal lies elsewhere than P680.

3.5. Quantification of oxidized electron donors in PSII during visible illumination at cryogenic temperatures

The results mentioned earlier have already shown that a similar amount of Split S_3 signal was induced regardless of whether the majority of centers were open or closed to P680-centered charge separation. This first indication of a P680-independent mechanism for the induction of the Split S_3 signal even in the visible region was then corroborated by quantifying the formation of the acceptor Q_A and the EPR-visible electron donors (Car, Chl and Cytb_{559}) that are involved in charge separation (see Materials and methods for the quantification procedure). If these donors alone are sufficient to account for the formation of the Q_A^-, then this would provide further evidence that Split S_3 formation is not related to P680-centered charge separation. The results are summarized in Table 2.

Without the pre-reduction of Q_A, Q_A^- was formed in ~90% of the centers when visible illumination at 5 K was applied. On the donor side, illumination led to the Cytb_{559} oxidation in ~60% of PSII, and Car/Chl oxidation in ~28% of centers (the radicals of these two species overlap almost exactly: [7]). Thus, the reduction of Q_A is well matched within our precision by the oxidation of the known electron donors from the Car/Chl/Cytb_{55} pathway. By contrast, the Split S_3 signal induced here was 96% of the maximum inducible intensity as obtained by NIR illumination in the absence of pre-formed Q_A^-.

In the case where Q_A^- was pre-formed before visible illumination at 5 K was applied, Q_A^- was formed in a total of 100% of the centers, of which ~70% was formed during the initial illumination at 77 K. In other words, only 30% of the Q_A^- reduced in total was reduced during the 5 K illumination. All oxidizable Cytb_{559} acceptors were oxidized also during this 77 K illumination step, accounting for ~60% of the donors. No extra Cytb_{559} oxidation was observed in the subsequent 5 K illumination. Car and Chl contributed to a total of ~38% of the donor species, of which ~13% was formed already in the Q_A^- reduction step at 77 K. As shown in Table 2, therefore, there was again a very good agreement between the amount of charge transfer acceptor and donor species that could be directly accounted for through quantification using EPR. Despite this good correspondence in acceptor and donor amounts, and the much lower amount of Q_A^- that was reduced during the split signal inducing 5 K illumination, the Split S_3 signal was nevertheless formed to 86% of the maximum inducible intensity. Clearly, not only are all acceptors and donors accounted for without the involvement of the split signal radical $Y_Z^\bullet$, there is also no correspondence between the decreases in the extent of Q_A reduction and the Split S_3 signal formation. This was also illustrated in the comparisons in Fig. 4. Combining the previously mentioned observations, therefore, it seems clear that the mechanism of Split S_3 signal formation does not involve charge separation originating from P680, even when induced with visible light.

Table 2
EPR quantification of acceptor and donor species induced by visible light illumination in samples (280 W/m^2) with and without pre-formed Q_A^-.

	Split S_3 signal intensity	Species		Amount induced (% PSII)	Of which induced at…[a]		Total (% PSII)
					77 K	5 K	
Visible illumination, Q_A^- not pre-formed	96% of maximum inducible intensity[b]	Acceptor	Q_A^-[c]	90	–	90	90
		Donors	Cytb_{559}[d]	60	–	60	88
			Car/Chl	28	–	28	
Visible illumination, Q_A^- pre-formed by 77 K illumination	86% of maximum inducible intensity[b]	Acceptor	Q_A^-[c]	100	70	30	100
		Donors	Cytb_{559}[d]	60	60	0	98
			Car/Chl	38	13	25	

[a] Estimated error (signal-to-noise) in quantification of signal intensity = ±3%. Reproducibility between duplicate samples: ±3% for Q_A^-, ±8% for Car/Chl induced by illumination at 5 K, and ±4% for Car/Chl induced by illumination at 77 K (i.e. the illumination used to pre-form Q_A^-).

[b] The maximum inducible intensity was obtained by NIR illumination at 5 K of a sample without pre-formed Q_A^- (see Fig. 1 and accompanying text). This represented ~52% of PSII centers.

[c] The maximum EPR signal from Q_A^--Fe^{2+} is set to represent reduced Q_A in 100% of PSII and was obtained in the sample illuminated *both* at 77 K and 5 K.

[d] In our PSII preparation ~60 ± 5% of Cytb_{559} is present in the reduced high-potential form from the start. All available reduced Cytb_{559} was photo-oxidized.

4. Discussion

The Split S_3 EPR signal can be induced by monochromatic light in the spectral range 415–900 nm [16]. The mechanistic explanation in the literature for the induction of the Split S_3 signal with NIR light involves excitation of a Mn(III) ion in the $CaMn_4$ cluster in the S_3 state, which then oxidizes the nearby Y_Z, thereby giving rise to the magnetic interaction signal [17,19,21,22]. The $CaMn_4$ cluster is thus reduced, giving a modified S_2 state assigned as S_2'. This mechanism is independent of charge separation originating from P680, which does not absorb in the NIR region. We have confirmed this in the current study. The NIR illumination generated no Q_A^--Fe^{2+} signal, and the resulting Split S_3 signal was stable in the dark at 5 K in the absence of pre-formed Q_A^- (Fig. 1B, black circles). By contrast, it decayed in the sample containing Q_A^- pre-formed via 77 K illumination (Fig. 3B, black circles). Therefore, the P680-independent origin of the Split S_3 signal was confirmed where NIR illumination was used. An important question is then whether the oxidation of Y_Z and the formation of the Split S_3 EPR signal in the visible light range involve charge separation driven from P680, or whether the same Mn-centered mechanism applies independent of the wavelength of the inducing light.

4.1. The formation of the Split S_3 EPR signal is not driven by P680 even in the visible part of the spectrum

We have made several observations that support this statement. First, quantitatively the same fraction of PSII centers could form the Split S_3 signal after saturating illumination both with NIR and visible light (Fig. 1A). Stronger support, however, comes from experiments in closed PSII with pre-reduced Q_A, which blocks the P680-driven charge separation leading to the oxidation of Y_Z. Here the amplitude of the Split S_3 signal was similar to where Q_A was oxidized (Table 2). This strongly supports a mechanism for the induction of the Split S_3 signal (and consequently for the oxidation of Y_Z) independent of P680-centered charge separation (dashed arrows in Scheme 1), and favors a Mn-centered mechanism for *both* the NIR and visible light induction of the Split S_3 signal (dotted arrows in Scheme 1). This can be contrasted with the Split S_1 signal. This signal has been shown to result from magnetic interaction between $Y_Z^\bullet$ and the $CaMn_4$ cluster

in the S_1 state, and it forms and decays in concert with Q_A reduction and re-oxidation [13,28], and is therefore driven by P680. As shown in Fig. 4, the pre-reduction of Q_A^- in S_1 state samples led to a much lower intensity Split S_1 state compared with the fully open sample with oxidized Q_A. The decrease in open (oxidized Q_A) centers due to prior formation of Q_A^- led to a much better correlation with the decrease in the yield of the Split S_1 signal. This is in stark contrast to our observations for the Split S_3 signal, where the split signal intensity was only marginally affected despite the presence of Q_A^- in 70% of the centers prior to 5 K illumination.

Attention can be drawn to another observation that strengthens our proposal that the Mn-centered mechanism is behind both the NIR and visible light induction of the Split S_3 signal formation. In both cases, illumination induces a derivative-shaped EPR signal that is observed in the $g=5$ region. The signal is stable in the dark (Fig. 2). This signal has previously been assigned to originate from the $CaMn_4$ cluster in the S_2' state resulting from the oxidation of Y_Z by the excited S_3 state cluster due to NIR irradiation: $S_3^* Y_Z \rightarrow S_2' Y_Z^\bullet$ [21,22,46]. The fact that this signal is also present after visible light illumination suggests that the $S_3 \rightarrow S_2'$ state conversion occurs even here. The induction of this $g\sim5$ signal by visible light has not been reported before. Its presence in both NIR and visible light illuminated samples adds further weight to our proposal that one and the same Mn-centered mechanism is behind Split S_3 signal formation for both illumination regimes.

Related to the presence of the $g\sim5/S_2'$ state signal in both visible and NIR illuminated samples is the observation that the spectral shape of the Split S_3 signal is independent of the light used for induction (after accounting for the presence of the overlapping Q_A^--Fe^{2+} signal for visible light illumination). As mentioned earlier, cryogenic NIR excitation of the $CaMn_4$ cluster in the S_3 state is expected to yield $S_2' Y_Z^\bullet$, the interacting paramagnetic pair giving rise to the Split S_3 signal. Now if visible illumination of the S_3 state were to give P680-driven oxidation of $Y_Z^\bullet$, the result would be as follows: $S_3\ Y_Z\ P680^* \rightarrow S_3\ Y_Z^\bullet$ P680. In that case, the resulting pair of paramagnetic centers giving rise to the Split S_3 signal would instead be $S_3 Y_Z^\bullet$. The S_3 state possesses one less electron than the S_2' state, and it is extremely unlikely that such two different paramagnetic pairs would give rise to split signals that are identical in their spectral shape, especially considering that there is significant structure in the signal, and that these signals would display the same microwave power saturation behavior [16]. Therefore, together with the presence of the $g\sim5$ signal in both NIR and visible light-induced Split S_3 signals, it is more reasonable that the same Mn-centered mechanism operates across the entire wavelength range.

To further corroborate these indications that seem to exclude P680-centered charge separation as the origin of the Split S_3 signal, we also quantified the total amount of Q_A^- formed and compare this to the amount of secondary donors to P680 that can be observed by EPR. As shown in Table 2, regardless of whether or not 77 K illumination was applied, the Q_A^- that was formed through illumination by visible light (i.e. via P680-centered charge separation) could be fully accounted for by the secondary donors Car, Chl and Cytb_{559}, without requiring contribution from the split radical $Y_Z^\bullet$. This demonstrated that the process generating the split radical $Y_Z^\bullet$ is independent of the charge separation process producing Q_A^-. Again, given the very small difference in the yield of the Split S_3 signal under these different starting conditions, it seems clear that the Mn-centered mechanism operates even in the visible light region.

From the data mentioned earlier, there is strong evidence for the mechanism for the induction of the Split S_3 signal being the same across the NIR and visible wavelength range. The same pattern of behavior was observed in at least four samples for each of the visible and NIR illumination regimes, and the quantification of donors and acceptors was performed on two independent samples. Nevertheless, we have observed some very intriguing and complex behavior in the induction and decay kinetics of the Split S_3 signals that are dependent upon the exact experimental conditions used. While the differences in induction kinetics between using visible and NIR light may at least partly be due to different absorption coefficients at these difference wavelengths [16] (note that standard filtered broad spectrum white light was used for visible illumination, whereas a 830 nm laser diode was used to ensure no contamination from visible light), the presence of pre-reduced Q_A^- appears to lead to faster induction kinetics when comparing within the different illumination regimes. The decay kinetics of the Split S_3 signal, reflecting the recombination of the Q_A^- with $S_2' Y_Z^\bullet$, is different for the NIR and visible light-induced signals. These effects may originate from structural, electrostatic and/or redox influences that the donor and acceptor sides of PSII can have on each other. A number of literature studies [47–49] have demonstrated that changes in the state of the donor side of PSII can lead to significant effects on the acceptor side, and vice versa. The two "ends" of the charge separation chain are not totally isolated from each other. Therefore, differences in the redox states of species such as Q_A, Chl, Car and Cytb_{559} in the different experiments here may have indeed had an effect on the induction and decay kinetics of the Split S_3 signal also. These are clearly interesting phenomena that warrant further and more focused investigations, with better time resolutions and further trials of different experimental conditions. This study is currently under way.

To summarize, the Split S_3 EPR signal can be induced by both visible and NIR light [16]. In neither case is charge separation originating from P680 (dashed arrows in Scheme 1) the photochemical origin of the signal. Rather, the Mn-centered mechanism operates for *both* visible and NIR light illumination (dotted arrows in Scheme 1), even where P680-centered charge separation can concurrently take place. The result was first indicated in a pre-study from our laboratory [50]. It has also been reported that the same split signal can be induced from the S_3 state using both NIR and visible light in PSII centers from *Thermosynechococcus elongatus*, even in the presence of Q_A^- [40].

4.2. Mn-driven formation of the Split S_3 EPR signal between 415 and 900 nm — extended "NIR sensitivity" in the S_3 state

This investigation shows that the formation of the Split S_3 signal, regardless of the wavelength of the inducing light (visible or NIR), is not driven by P680-centered charge separation. Instead our results indicate that the same type of photochemistry, most probably involving excitation of a Mn ion in the $CaMn_4$ cluster, occurs irrespective of the illumination regime. The simplest explanation is that the relevant absorption band(s) from this Mn ion stretches over the entire 415–900 nm interval [16]. The Mn photochemistry induced in the S_3 state includes the visible as well as the NIR light range, hence it can be seen as an extended "NIR sensitivity".

NIR sensitivity for S_2 state of the $CaMn_4$ cluster has been attributed to a Mn(III) ion [51–54], partly based on circumstantial evidence relating the NIR-effect observed in PSII to a NIR MCD band that is assigned to the Mn(III) ion in a Mn(III,IV) complex [55]. This assignment holds for both the S_2 and S_3 states due to the similar action spectra of NIR-induced transitions in the 720–860 nm region [19]. One reason that Mn(III) has been favored as the site of NIR absorption [52] is that in an octahedral ligand field, the d^4 configuration would give rise to Jahn–Teller distortion. For centrosymmetric complexes, this is an important distinction from Mn(IV)/d^3, as the Jahn–Teller distortion would mean that d–d transitions are no longer Laporte (parity) forbidden, thereby allowing for stronger absorptions ($\varepsilon\sim100$–$1000\ L\ mol^{-1}\ cm^{-1}$). Depending on the distortion and the ligand field strength of the ligands, these transitions could be in the NIR region. By contrast, the lack of Jahn–Teller distortion means that there would be no appreciable absorption due to d–d transitions in (centrosymmetric) Mn(IV) complexes.

Following this logic, if only Mn(III) and not Mn(IV) were NIR sensitive, then the observation of NIR sensitivity in the S_3 states would suggest that there is at least one Mn(III) ion present in this state. Assuming that the S_2 state of the cluster consist of Mn ions in the oxidation states (III,IV,IV,IV) [56], this requirement of the existence of a Mn(III) ion in the S_3 state would imply that the only Mn(III) ion present in the S_2 state remains unoxidized upon progression to the S_3 state. This would therefore imply that there is a ligand-centered oxidation during the $S_2 \rightarrow S_3$ transition, rather than a Mn-oxidation. This is controversial, since the site of oxidation (Mn *vs.* a ligand of the $CaMn_4$ cluster) during this transition is still far from settled, despite numerous attempts to resolve this issue using various X-ray spectroscopic techniques [57–59]. It is also a central question touching upon the mechanism of the water oxidation mechanism. However, for two sets of reasons, we do not believe that the observed NIR sensitivity in the S_3 state necessarily implies the presence of a Mn(III) ion.

Firstly, even if it was reasonable to consider each Mn ion in the cluster individually and independently of the other ions, the ligand environment of the Mn ions in the $CaMn_4$ cluster is far from perfectly octahedral, let alone centrosymmetric. As such, metal-centered d–d transitions are not formally Laporte forbidden, regardless of whether the ion is Mn(III)/d^4 or Mn(IV)/d^3. There is no reason to favor one over the other as the absorbing species. For instance, a mononuclear octahedral Mn(IV) complex lacking centrosymmetry has been shown to exhibits absorption bands at 800, 550 and 500 nm, corresponding to three d–d transitions [60]. Furthermore, for MLCT, LMCT and intervalent charge transfers, a more careful analysis of the symmetries of the ground and resulting excited state is required, to include the ligand or other ion involved in the charge transfer. As such, a simple application of the Laporte selection rule to exclude the involvement of the Mn(IV) ions is not possible.

Many mononuclear Mn(III) and Mn(IV) complexes [60–62], binuclear Mn(III,III) [63] and Mn(III,IV) complexes [55,64], as well as a tetranuclear $Mn(IV)_4$ complex [65] show a multitude of absorption bands and MCD features over the entire 400–900 nm region. In particular, a number of binuclear Mn(III,IV) and Mn(IV, IV) complexes containing a di-μ-oxo bridged Mn_2O_2 core, a motif that is also found in the $CaMn_4$ cluster, exhibit very broad absorption spectra, spanning the 300–1500 nm range [55,66,67]. The numerous optical features have variously been assigned to transitions involving metal-centered d–d transitions, oxo-to-metal charge transfer transitions and intervalence transfer transitions. An especially interesting illustration of the pitfall of equating NIR sensitivity with Mn(III) is a binuclear Mn complex that shows no NIR absorption in the Mn(III, IV) state, but does absorb NIR radiation in the Mn(IV, IV) state [66].

The second reason is closely related to the examples of binuclear Mn complexes mentioned earlier. Given the extensive oxo bridging between the Mn ions within the cluster, it is probably not reasonable to neglect the electronic coupling between ions. In other words, it is not sufficient to regard the cluster in terms of four independent Mn ions when considering its electronic structure. A significant degree of electronic delocalization is likely to be present, which would clearly affect the absorption spectrum of the cluster. Good descriptions of the categorization of polynuclear mixed-valence metal complexes into classes I, II and III depending on the extent of coupling and their respective spectroscopic characteristics can be found in the literature [68,69]. Particularly relevant to the $CaMn_4$ is the class II category, where the coupling is not so strong such that the ions are indistinguishable and give spectra unrelated to their component ions (class III), or so weak that they are independent of each of other (class I) and give spectra that are simply superpositions of the component ions' spectra. In this intermediate class II case, coupling is strong enough to give interaction between the ions and a certain degree of electronic delocalization, but the ions are still distinguishable.

The classification of the $CaMn_4$ as a class II-type mixed-valent polynuclear complex can be justified by the ample EPR and theoretical studies of the $CaMn_4$ cluster which have demonstrated that not only are the Mn ions exchange coupled to each other to different degrees, the couplings also vary across the S-cycle. Furthermore, the hyperfine interaction parameters, spin and charge density distributions and spin projections are not equal across the Mn ions in the cluster, even for ions with the same formal oxidation state [56,70,71]. This further argues for a significant degree of delocalization across the cluster, but with the ions nevertheless being distinguishable from each other, especially given the inherent asymmetry within the $CaMn_4$ cluster. (See also the classification of di-μ-oxo bridged binuclear Mn complexes as class II in [64].)

Due to the coupling between the ions, the spectra from such class II complexes exhibit characteristics of the individual ions, but also extra features as a result of the coupling between ions [68,69]. This may explain the broad excitation range of the cluster in the S_3 state. Considering the different ligation motifs for the different Mn ions (both from amino acid ligands and μ-oxo bridging within the cluster), there may be a large number of overlapping bands across a wide wavelength range. Clearly the energy required for electronic transitions are sensitive to the ligand environment. Therefore, while individual absorption bands may not be broad enough to cover the full spectral range, there may be enough overlapping bands across the visible and NIR range to give rise to excitation of the $CaMn_4$ cluster.

Therefore, regardless of whether the Mn ions in $CaMn_4$ are considered as independent ion complexes, the involvement of Mn(IV) ion(s) in the excitation of the cluster in the S_3 state leading to the Split S_3 signal formation remains a possibility. The presence of a Mn(III) ion in the S_3 state is neither an absolute requirement nor necessarily excluded. As such, the present observation of the broad visible and NIR sensitivity of the S_3 state in the induction of the Split S_3 signal remains compatible with either a ligand-centered or a Mn-centered oxidation mechanism for the $S_2 \rightarrow S_3$ state transition, and the involvement of Mn(IV) species is a possibility.

5. Conclusions

ModernThe Split S_3 signal can be induced in PSII samples in the S_3 state by illumination with NIR and visible light at 5 K. By comparing the induction and decay characteristics of this signal both in the presence and in the absence of pre-formed Q_A^- in the sample prior to split signal inducing illumination, it was concluded that the Split S_3 signal formed independent of P680-centered charge separation. In particular, it was found that this was true not only for NIR illumination, but also for the Split S_3 signal induction using visible light. This was an unexpected and novel finding. It suggests that for both visible and NIR illumination of S_3 state samples at 5 K, charge separation originating from P680 is not involved in the oxidation of the radical interacting with the $CaMn_4$ cluster to give the Split S_3 signal, namely $Y_Z^{\bullet}$. Rather, direct excitation of Mn in the $CaMn_4$ in the S_3 state may operate even for the visible light range, in the same manner as proposed for NIR illumination.

Particularly strong evidence for this was the lack of correspondence between the amount of centers closed to P680-charge separation due to the presence of Q_A^-, and the intensity of the Split S_3 signal that could be induced. Even with ~70% of PSII centers in the closed state prior to the induction of the split signal with visible light, the Split S_3 signal intensity only decreased by 10%. This could be contrasted with the case of the Split S_1 signal, where a much better correlation was observed. Furthermore, for the S_3 state, the amount of Q_A^- reduction observed after split signal inducing illumination could be completely accounted for by the electron donors Chl, Car and Cytb_{559}, both in samples with or without pre-formed Q_A^-. Again, this indicates that Split S_3 signal induction is independent of P680-centered charge separation.

A stable $g \sim 5$ signal was observed after the induction of the Split S_3 signal, for both visible and NIR illumination regimes. This $g \sim 5$ signal has previously reported in the literature for NIR illumination of the S_3

state, and has been attributed to a $S_3 \rightarrow S_2'$ state transition due to the oxidation of Y_Z to $Y_Z^\bullet$ by an excited S_3 state $CaMn_4$ cluster. The observation of this $g \sim 5$ signal even in samples illuminated with visible light suggests that one and the same Mn-centered mechanism operates for the induction of the Split S_3 signal, regardless of the light used.

We therefore propose that the Split S_3 EPR signal, hence the $Y_Z^\bullet$ radical, is formed via excitation of a Mn ion, independent of the wavelength of the inducing light in the range 415–900 nm. While this has been thought to involve the excitation of a Mn(III) ion in the $CaMn_4$ cluster, a more careful consideration of the symmetry ligand environment around the Mn ions in the $CaMn_4$ cluster suggests that either Mn(III) or Mn(IV) can be the light-sensitive species. Indeed, considerations of the coupling between the constitutive Mn ions of the cluster suggests that one should move beyond a localized identification of a single absorbing ion, and factor in the more complex electronic structure of the mixed-valent polynuclear complex that the $CaMn_4$ cluster is.

Acknowledgements

The authors would like to thank Jean-Jacques Girerd, Elmars Krauz, Ron Pace, Anders Thapper, Johannes Sjöholm, Gustav Berggren and Reiner Lomoth for helpful discussions. The Swedish Research Council, the Swedish Energy Agency, the Knut and Alice Wallenberg Foundation, the EU program SOLAR-H2 (EU contract 212508), the Carl Tryggers Foundation for Scientific Research (to F.M.H.) and the Nordic Energy Research Program 06-Hydr-C13 (to K.G.V.H.) are gratefully acknowledged for financial support.

References

[1] A.W. Rutherford, Photosystem II, the water-splitting enzyme, Trends Biochem. Sci. 14 (1989) 227–232.
[2] J. Barber, Photosystem II: the engine of life, Q. Rev. Biophys. 36 (2003) 71–89.
[3] N. Nelson, C.F. Yocum, Structure and function of photosystems I and II, Annu. Rev. Plant Biol. 57 (2006) 521–565.
[4] D.A. Force, D.W. Randall, R.D. Britt, X.S. Tang, B.A. Diner, ^{2}H ESE-ENDOR study of hydrogen bonding to the tyrosine radicals Y_D and Y_Z of photosystem II, J. Am. Chem. Soc. 117 (1995) 12643–12644.
[5] C. Tommos, X.S. Tang, K. Warncke, C.W. Hoganson, S. Styring, J. McCracken, B.A. Diner, G.T. Babcock, Spin-density distribution, conformation, and hydrogen-bonding of the redox-active tyrosine Y_Z in photosystem II from multiple electron magnetic-resonance spectroscopies: implications for photosynthetic oxygen evolution, J. Am. Chem. Soc. 117 (1995) 10325–10335.
[6] A.W. Rutherford, A. Boussac, P. Faller, The stable tyrosyl radical in photosystem II: why D? Biochim. Biophys. Acta 1655 (2004) 222–230.
[7] J. Hanley, Y. Deligiannakis, A. Pascal, P. Faller, A.W. Rutherford, Carotenoid oxidation in photosystem II, Biochemistry 38 (1999) 8189–8195.
[8] C.A. Tracewell, A. Cua, D.H. Stewart, D.F. Bocian, G.W. Brudvig, Characterization of carotenoid and chlorophyll photooxidation in photosystem II, Biochemistry 40 (2001) 193–203.
[9] H.A. Frank, G.W. Brudvig, Redox functions of carotenoids in photosynthesis, Biochemistry 43 (2004) 8607–8615.
[10] S. Styring, A.W. Rutherford, Deactivation kinetics and temperature-dependence of the S-state transitions in the oxygen-evolving system of photosystem II measured by EPR spectroscopy, Biochimica. et. Biophysica. Acta 933 (1988) 378–387.
[11] K. Brettel, E. Schlodder, H.T. Witt, Nanosecond reduction kinetics of photooxidized chlorophyll-a_{II} (P-680) in single flashes as a probe for the electron pathway, H^+-release and charge accumulation in the O_2-evolving complex, Biochim. Biophys. Acta 766 (1984) 403–415.
[12] C.W. Hoganson, G.T. Babcock, Electron-transfer events near the reaction center in O_2-evolving photosystem-II preparations, Biochemistry 27 (1988) 5848–5855.
[13] J.H. Nugent, I.P. Muhiuddin, M.C. Evans, Electron transfer from the water oxidizing complex at cryogenic temperatures: the S_1 to S_2 step, Biochemistry 41 (2002) 4117–4126.
[14] J.H. Nugent, S. Turconi, M.C. Evans, EPR investigation of water oxidizing photosystem II: detection of new EPR signals at cryogenic temperatures, Biochemistry 36 (1997) 7086–7096.
[15] V. Petrouleas, D. Koulougliotis, N. Ioannidis, Trapping of metalloradical intermediates of the S-states at liquid helium temperatures. Overview of the phenomenology and mechanistic implications, Biochemistry 44 (2005) 6723–6728.
[16] J.H. Su, K.G.V. Havelius, F.M. Ho, G. Han, F. Mamedov, S. Styring, Formation spectra of the EPR split signals from the S_0, S_1, and S_3 states in photosystem II induced by monochromatic light at 5 K, Biochemistry 46 (2007) 10703–10712.
[17] N. Ioannidis, V. Petrouleas, Electron paramagnetic resonance signals from the S_3 state of the oxygen-evolving complex. A broadened radical signal induced by low-temperature near-infrared light illumination, Biochemistry 39 (2000) 5246–5254.
[18] D. Koulougliotis, J.R. Shen, N. Ioannidis, V. Petrouleas, Near-IR irradiation of the S_2 state of the water oxidizing complex of photosystem II at liquid helium temperatures produces the metalloradical intermediate attributed to S_1Y_Z*, Biochemistry 42 (2003) 3045–3053.
[19] A. Boussac, M. Sugiura, D. Kirilovsky, A.W. Rutherford, Near-infrared-induced transitions in the manganese cluster of photosystem II: action spectra for the S_2 and S_3 redox states, Plant Cell Physiol. 46 (2005) 837–842.
[20] J.L. Hughes, P. Smith, R. Pace, E. Krausz, Charge separation in photosystem II core complexes induced by 690–730 nm excitation at 1.7 K, Biochim. Biophys. Acta 1757 (2006) 841–851.
[21] N. Ioannidis, J.H. Nugent, V. Petrouleas, Intermediates of the S_3 state of the oxygen-evolving complex of photosystem II, Biochemistry 41 (2002) 9589–9600.
[22] N. Ioannidis, V. Petrouleas, Decay products of the S_3 state of the oxygen-evolving complex of photosystem II at cryogenic temperatures. Pathways to the formation of the $S = 7/2$ S_2 state configuration, Biochemistry 41 (2002) 9580–9588.
[23] D.A. Berthold, G.T. Babcock, C.F. Yocum, A highly resolved, oxygen-evolving photosystem II preparation from spinach thylakoid membranes, FEBS Lett. 134 (1981) 231–234.
[24] M. Völker, T. Ono, Y. Inoue, G. Renger, Effect of trypsin on PS II particles: correlation between Hill-activity. Mn-abundance and peptide pattern, Biochimica Et Biophysica Acta 806 (1985) 25–34.
[25] D.I. Arnon, Copper enzymes in isolated chloroplasts. Polyphenoloxidase in *Beta Vulgaris*, Plant Physiology 24 (1949) 1–15.
[26] S. Styring, A.W. Rutherford, In the oxygen-evolving complex of photosystem II the S_0 state is oxidized to the S_1 state by D^+ (Signal-II_{slow}), Biochemistry 26 (1987) 2401–2405.
[27] G. Han, F.M. Ho, K.G.V. Havelius, S.F. Morvaridi, F. Mamedov, S. Styring, Direct quantification of the four individual S states in photosystem II using EPR spectroscopy, Biochim. Biophys. Acta 1777 (2008) 496–503.
[28] C. Zhang, A. Boussac, A.W. Rutherford, Low-temperature electron transfer in photosystem II: a tyrosyl radical and semiquinone charge pair, Biochemistry 43 (2004) 13787–13795.
[29] Y. Feyziyev, B.J. van Rotterdam, G. Bernat, S. Styring, Electron transfer from cytochrome b_{559} and tyrosine$_D$ to the S_2 and S_3 states of the water oxidizing complex in photosystem II, Chem. Phys. 294 (2003) 415–431.
[30] D.H. Stewart, G.W. Brudvig, Cytochrome b559 of photosystem II, Biochim. Biophys. Acta 1367 (1998) 63–87.
[31] M. Roncel, J.M. Ortega, M. Losada Factors, determining the special redox properties of photosynthetic cytochrome b_{559}, Eur. J. Biochem. 268 (2001) 4961–4968.
[32] F. Mamedov, R. Danielsson, R. Gadjieva, P.-Å. Albertsson, S. Styring, EPR characterization of photosystem II from different domains of the thylakoid membrane, Biochemistry 47 (2008) 3883–3891.
[33] P. Faller, C. Fufezan, A.W. Rutherford, Side path electron donors: cytochrome $_{b559}$, chlorophyll Z and β-carotene, in: T. Wydrzynski, K. Satoh (Eds.), Photosystem II: the Light-Driven Water:Plastoquinone Oxidoreductase, Springer, Dordrecht, 2005, pp. 347–365.
[34] A.-F. Miller, G.W. Brudvig, A guide to electron paramagnetic resonance spectroscopy of photosystem II membranes, Biochim. Biophys. Acta 1056 (1991) 1–18.
[35] A. Garbers, R. Frank, J. Kurreck, G. Renger, F. Parak, Correlation between protein flexibility and electron transfer from Q_A-• to Q_B in PSII membrane fragments from spinach, Biochemistry 37 (1998) 11399–11404.
[36] F. Reifarth, G. Renger, Indirect evidence for structural changes couple with Q_B-• formation in photosystem II, FEBS Lett. 428 (1998) 123–126.
[37] C. Fufezan, C. Zhang, A. Krieger-Liszkay, A.W. Rutherford, Secondary quinone in photosystem II of *Thermosynechococcus elongatus*: semiquinone-iron EPR signals and temperature dependence of electron transfer, Biochemistry 44 (2005) 12780–12789.
[38] J.H.A. Nugent, B.A. Diner, M.C.W. Evans, Direct detection of the electron acceptor of photosystem II: evidence that Q is an iron–quinone complex, FEBS Lett. 124 (1981) 241–244.
[39] A.W. Rutherford, J.L. Zimmermann, A new EPR signal attributed to the primary plastosemiquinone acceptor in photosystem II, Biochim. Biophys. Acta 767 (1984) 168–175.
[40] A. Boussac, M. Sugiura, T.L. Lai, A.W. Rutherford, Low-temperature photochemistry in photosystem II from *Thermosynechococcus elongatus* induced by visible and near-infrared light, Philos. Trans. R. Soc. London. Ser. B. 363 (2008) 1203–1210.
[41] K.G.V. Havelius, J.H. Su, Y. Feyziyev, F. Mamedov, S. Styring, Spectral resolution of the split EPR signals induced by illumination at 5 K from the S_1, S_3, and S_0 states in photosystem II, Biochemistry 45 (2006) 9279–9290.
[42] K.G.V. Havelius, J. Sjöholm, F.M. Ho, F. Mamedov, S. Styring, Metalloradical EPR signals from the $Y_Z^\bullet$ S-state intermediates in photosystem II, Appl. Magn. Reson. 37 (2010) 151–176.
[43] G. Sioros, D. Koulougliotis, G. Karapanagos, V. Petrouleas, The $S_1Y_Z^\bullet$ metalloradical EPR signal of photosystem II contains two distinct components that advance respectively to the multiline and $g = 4.1$ conformations of S_2, Biochemistry 46 (2007) 210–217.
[44] N. Ioannidis, G. Zahariou, V. Petrouleas, The EPR spectrum of tyrosine $Z^\bullet$ and its decay kinetics in O_2-evolving photosystem II preparations, Biochemistry 47 (2008) 6292–6300.
[45] N. Cox, F.M. Ho, N. Pewnim, R. Steffen, P.J. Smith, K.G.V. Havelius, J.L. Hughes, L. Debono, S. Styring, E. Krausz, R.J. Pace, The S_1 split signal of photosystem II; a

tyrosine-manganese coupled interaction, Biochim. Biophys. Acta 1787 (2009) 882–889.
[46] Y. Sanakis, N. Ioannidis, G. Sioros, V. Petrouleas, A novel S = 7/2 configuration of the Mn cluster of photosystem II, J. Am. Chem. Soc. 123 (2001) 10766–10767.
[47] G.N. Johnson, A.W. Rutherford, A. Krieger, A change in the midpoint potential of the quinone Q_A in photosystem II associated with photoactivation of oxygen evolution, Biochim. Biophys. Acta 1229 (1995) 202–207.
[48] H. Bao, C. Zhang, K. Kawakami, Y. Ren, J.-R. Shen, J. Zhao, Acceptor side effects on the electron transfer at cryogenic temperatures in intact photosystem II, Biochim. Biophys. Acta 1777 (2008) 1109–1115.
[49] H. Bao, C. Zhang, Y. Ren, J. Zhao, Low-temperature electron transfer suggests two types of Q_A in intact photosystem II, Biochim. Biophys. Acta 1797 (2010) 339–346.
[50] K.G.V. Havelius, J.-H. Su, F.M. Ho, G. Han, F. Mamedov, S. Styring, The mechanism behind the formation of the "Split S_3" EPR signal in photosystem II induced by visible or near-infrared light, in: J.F. Allen, E. Gantt, J.H. Golbeck, B. Osmond (Eds.), Photosysnthesis. Energy From the Sun: 14th International Congress on Photosynthesis, vol. 1, Springer, Glasgow, 2007, pp. 423–426.
[51] A. Boussac, J.J. Girerd, A.W. Rutherford, Conversion of the spin state of the manganese complex in photosystem II induced by near-infrared light, Biochemistry 35 (1996) 6984–6989.
[52] R. Baxter, E. Krausz, T. Wydrzynski, R.J. Pace, Identification of the near-infrared absorption band from the Mn cluster of photosystem II, J. Am. Chem. Soc. 121 (1999) 9451–9452.
[53] O. Horner, E. Riviere, G. Blondin, S. Un, A.W. Rutherford, J.J. Girerd, A. Boussac, SQUID magnetization study of the infrared-induced spin transition in the S_2 state of photosystem II: spin value associated with the $g = 4.1$ EPR signal, J. Am. Chem. Soc. 120 (1998) 7924–7928.
[54] D. Kuzek, R.J. Pace, Probing the Mn oxidation states in the OEC. Insights from spectroscopic, computational and kinetic data, Biochim. Biophys. Acta 1503 (2001) 123–137.
[55] D.R. Gamelin, M.L. Kirk, T.L. Stemmler, S. Pal, W.H. Armstrong, J.E. Pennerhahn, E.I. Solomon, Electronic-structure and spectroscopy of manganese catalase and di-μ-oxo [Mn(III)Mn(IV)] model complexes, J. Am. Chem. Soc. 116 (1994) 2392–2399.
[56] L.V. Kulik, B. Epel, W. Lubitz, J. Messinger, Electronic structure of the Mn_4O_xCa cluster in the S_0 and S_2 states of the oxygen-evolving complex of photosystem II based on pulse ^{55}Mn-ENDOR and EPR spectroscopy, J. Am. Chem. Soc. 129 (2007) 13421–13435.
[57] H. Dau, M. Haumann, The manganese complex of photosystem II in its reaction cycle — basic framework and possible realization at the atomic level, Coord. Chem. Rev. 252 (2008) 273–295.
[58] M. Haumann, C. Müller, P. Liebisch, L. Iuzzolino, J. Dittmer, M. Grabolle, T. Neisius, W. Meyer-Klaucke, H. Dau, Structural and oxidation state changes of the photosystem II manganese complex in four transitions of the water oxidation cycle ($S_0 \rightarrow S_1$, $S_1 \rightarrow S_2$, $S_2 \rightarrow S_3$, and $S_{3,4} \rightarrow S_0$) characterized by X-ray absorption spectroscopy at 20 K and room temperature, Biochemistry 44 (2005) 1894–1908.
[59] J. Messinger, J.H. Robblee, U. Bergmann, C. Fernandez, P. Glatzel, H. Visser, R.M. Cinco, K.L. McFarlane, E. Bellacchio, S.A. Pizarro, S.P. Cramer, K. Sauer, M.P. Klein, V.K. Yachandra, Absence of Mn-centered oxidation in the $S_2 \rightarrow S_3$ transition: implications for the mechanism of photosynthetic water oxidation, J. Am. Chem. Soc. 123 (2001) 7804–7820.
[60] R. Mukhopadhyay, S. Bhattacharjee, C.K. Pal, S. Karmakar, R. Bhattacharyya, Generation of manganese-(III) versus -(IV) complexes with a conjugated ONS donor set: controlling effect of ligand substituents, J. Chem. Soc. Dalton Trans. 1 (1997) 2267–2272.
[61] S. Romain, C. Baffert, C. Duboc, J.C. Lepretre, A. Deronzier, M.N. Collomb, Mononuclear Mn^{III} and Mn^{IV} bis-terpyridine complexes: electrochemical formation and spectroscopic characterizations, Inorg. Chem. 48 (2009) 3125–3131.
[62] J. Shen, M. El Ojaimi, M. Chkounda, C.P. Gros, J.M. Barbe, J. Shao, R. Guilard, K.M. Kadish, Solvent, anion, and structural effects on the redox potentials and UV–visible spectral properties of mononuclear manganese corroles, Inorg. Chem. 47 (2008) 7717–7727.
[63] J.E. Sheats, R.S. Czernuszewicz, G.C. Dismukes, A.L. Rheingold, V. Petrouleas, J. Stubbe, W.H. Armstrong, R.H. Beer, S.J. Lippard, Binuclear manganese(III) complexes of potential biological significance, J. Am. Chem. Soc. 109 (1987) 1435–1444.
[64] S.R. Cooper, M. Calvin, Mixed-valence interactions in di-μ-oxo bridged manganese complexes, J. Am. Chem. Soc. 99 (1977) 6623–6630.
[65] C. Philouze, G. Blondin, J.J. Girerd, J. Guilhem, C. Pascard, D. Lexa, Aqueous chemistry of high-valent manganese. Structure, magnetic, and redox properties of a new type of Mn-oxo cluster, $[(Mn^{IV}{}_4O_6(bpy)_6]^{4+}$: relevance to the oxygen evolving center in plants, J. Am. Chem. Soc. 116 (1994) 8557–8565.
[66] M. Suzuki, S. Tokura, M. Suhara, A. Uehara, Dinuclear manganese(iii, iv) and manganese(iv, iv) complexes with tris(2-pyridylmethyl)amine, Chem. Lett. 17 (1988) 477–480.
[67] P.A. Goodson, J. Glerup, D.J. Hodgson, K. Michelsen, E. Pedersen, Binuclear bis(μ-oxo)dimanganese(III,IV) and bis(μ-oxo)dimanganese(IV,IV) complexes with *N,N′*-bis(2-pyridylmethyl)-1,2-ethanediamine, Inorg. Chem. 29 (1990) 503–508.
[68] M.B. Robin, P. Day, Mixed valence chemistry — a survey and classification, Adv. Inorg. Chem. Radiochem. 10 (1967) 248–422.
[69] V. Balzani, A. Juris, M. Venturi, S. Campagna, S. Serroni, Luminescent and redox-active polynuclear transition metal complexes, Chem. Rev. 96 (1996) 759–833.
[70] E.M. Sproviero, J.A. Gascon, J.P. McEvoy, G.W. Brudvig, V.S. Batista, Computational studies of the O_2-evolving complex of photosystem II and biomimetic oxomanganese complexes, Coord. Chem. Rev. 252 (2008) 395–415.
[71] D.A. Pantazis, M. Orio, T. Petrenko, S. Zein, W. Lubitz, J. Messinger, F. Neese, Structure of the oxygen-evolving complex of photosystem II: information on the S_2 state through quantum chemical calculation of its magnetic properties, Phys. Chem. Chem. Phys. 11 (2009) 6788–6798.